Near-zero-index media as electromagnetic ideal fluids

Iñigo Liberal[a,b,1,2], Michaël Lobet[c,1], Yue Li[d], and Nader Engheta[e,2]

[a]Electrical and Electronic Engineering Department, Universidad Pública de Navarra, Pamplona 31006, Spain; [b]Institute of Smart Cities, Universidad Pública de Navarra, Pamplona 31006, Spain; [c]Centre Spatial de Liège, Space sciences, Technologies and Astrophysics Research (STAR) Institute, University of Liege, B-4031 Angleur, Belgium; [d]Department of Electronic Engineering, Tsinghua University, Beijing 100084, China; and [e]Department of Electrical and Systems Engineering, University of Pennsylvania, Philadelphia, PA 19104

Edited by Stephen R. Forrest, University of Michigan, Ann Arbor, MI, and approved July 31, 2020 (received for review April 29, 2020)

Near-zero-index (NZI) supercoupling, the transmission of electromagnetic waves inside a waveguide irrespective of its shape, is a counterintuitive wave effect that finds applications in optical interconnects and engineering light–matter interactions. However, there is a limited knowledge on the local properties of the electromagnetic power flow associated with supercoupling phenomena. Here, we theoretically demonstrate that the power flow in two-dimensional (2D) NZI media is fully analogous to that of an ideal fluid. This result opens an interesting connection between NZI electrodynamics and fluid dynamics. This connection is used to explain the robustness of supercoupling against any geometrical deformation, to enable the analysis of the electromagnetic power flow around complex geometries, and to examine the power flow when the medium is doped with dielectric particles. Finally, electromagnetic ideal fluids where the turbulence is intrinsically inhibited might offer interesting technological possibilities, e.g., in the design of optical forces and for optical systems operating under extreme mechanical conditions.

near-zero-index media | metamaterials | nanophotonics | fluid dynamics

One of the most iconic and fascinating effects related to near-zero-index (NZI) media (1–4) is supercoupling (5), i.e., the perfect transmission of electromagnetic waves through a deformed waveguide, with zero phase advance, and independently of the geometry of the deformation. In fact, it was one of the first effects to be discovered and demonstrated, and it is a very good example of how NZI media lead to qualitatively different dynamics (6), often of a geometry-invariant nature (7). NZI supercoupling has been experimentally demonstrated in different waveguide configurations (8–16). In addition, supercoupling has been proposed for multiple applications, including waveguide interconnects (16), enhanced nonlinearities (17, 18), sensing (19), antennas (20–22), lenses (23, 24), enhanced fluorescence (25), quantum emission (26–28), control of dipole–dipole interactions (29), and entanglement generation (30, 31). The extension of this effect to other physical systems, including acoustic (32, 33) and electron (34) waves, has also been investigated.

However, despite the vast research activities around NZI supercoupling, less attention has been paid to the characteristics of the internal power flow associated to such effect. It has been extensively reported that the power does indeed flow between both waveguide ends, but, strikingly, the microscopic details of the power flow have been left unexplored. In other words, there is less knowledge on how the electromagnetic power actually flows within the waveguide and how this flow is modified as the waveguide is deformed. Fig. 1 shows a typical example of the power flow distribution in a deformed two-dimensional (2D) waveguide at the NZI frequency. For the sake of comparison, we report the power flow in the same geometry, but when resonant transmission (35) is achieved by finely tuning the relative permittivity of a dielectric material filling the waveguide to $\varepsilon = 6.42$ (while the relative permeability is kept at $\mu = 1$). These numerical results suggest that the power flow in NZI supercoupling is unusually simple and organized, smoothly adapting to the waveguide geometry. By contrast with resonant dielectric transmission, there are no whirlpools in the power flow. In fact, the power flow locally changes its direction, but it seems that it never points against the incident direction inside the NZI waveguide. Here, we shed light on the characteristics of this peculiar effect by theoretically investigating the local power flow in NZI media. In particular, we theoretically demonstrate that the power flow in 2D NZI media is equivalent to the flow of an inviscid, incompressible, and irrotational fluid, usually referred to as an ideal fluid (36–38).

Power Flow in 2D NZI Media

We start by considering the electromagnetic power flow within an isotropic medium characterized by a complex relative permittivity $\varepsilon = \varepsilon' + i\varepsilon''$ and permeability $\mu = \mu' + i\mu''$. An $e^{-i\omega t}$ time convention is assumed and omitted hereafter. For mathematical convenience, we consider the time-averaged complex Poynting vector field, $\mathbf{S} = \mathbf{S}_R + i\mathbf{S}_I = \frac{1}{2}\,\mathbf{E} \times \mathbf{H}^*$, where the real part $\mathbf{S}_R$ characterizes the time-averaged power flow, while the imaginary part $\mathbf{S}_I$ relates to reactive power flow that does not contribute to the net power passing through the waveguide. First, outside the source region the divergence of $\mathbf{S}$ is given by

$$\nabla \cdot \mathbf{S} = -\frac{\omega}{2}\left[\left(\varepsilon_0 \varepsilon'' \left|\mathbf{E}\right|^2 + \mu_0 \mu'' \left|\mathbf{H}\right|^2\right) + i\left(\varepsilon_0 \varepsilon' \left|\mathbf{E}\right|^2 - \mu_0 \mu' \left|\mathbf{H}\right|^2\right)\right]. \quad [1]$$

It is clear from Eq. **1** that the real part is zero for any lossless media ($\mu'', \varepsilon'' \to 0$). This conclusion simply points to the fact

Significance

Similar to turbulent fluid flow, irregular fluctuations and vortexes appear as light encounters obstacles. However, the properties of light dramatically change when it propagates within materials with extreme parameters, for example, a near-zero refractive index. Here, we demonstrate that the electromagnetic power flow in near-zero-index (NZI) media is fully analogous to the velocity field of an ideal fluid. In other words, NZI media act as electromagnetic ideal fluids where the turbulence of light is intrinsically inhibited. This result connects the fields of nanophotonics and fluid dynamics, opening interesting questions from both fundamental and technological perspectives.

Author contributions: I.L., M.L., and N.E. designed research; I.L. and M.L. performed research; I.L., M.L., Y.L., and N.E. analyzed data; and I.L., M.L., Y.L., and N.E. wrote the paper.

The authors declare no competing interest.

This article is a PNAS Direct Submission.

Published under the PNAS license.

[1]I.L. and M.L. contributed equally to this work.

[2]To whom correspondence may be addressed. Email: inigo.liberal@unavarra.es or engheta@seas.upenn.edu.

This article contains supporting information online at https://www.pnas.org/lookup/suppl/doi:10.1073/pnas.2008143117/-/DCSupplemental.

Downloaded at Tsinghua Univ Library on September 10, 2020

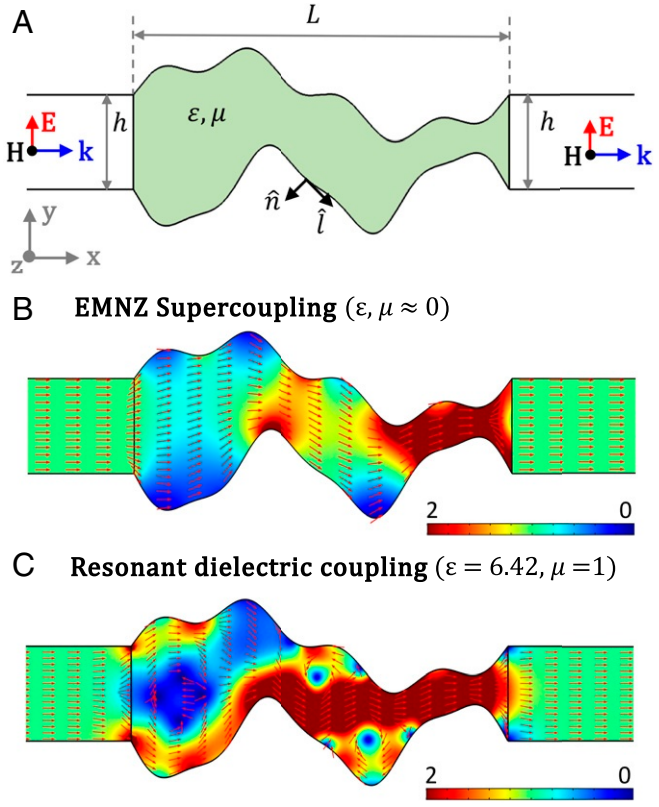

Fig. 1. (*A*) Sketch of the geometry: a 2D waveguide of height $h = 0.25\lambda$ containing a deformed section of length $L = \lambda$, filled with a material with relative permittivity ε and permeability μ. λ is the free-space wavelength at the frequency of the incoming wave. $\hat{\mathbf{n}}$ and $\hat{\mathbf{l}}$ are the normal and tangential unit vectors to the boundary of the NZI region, respectively. (*B* and *C*) Amplitude and normalized vector plot of the real part of the Poynting vector field ($\mathbf{S}_R$, power flow) when the waveguide is filled with (*B*) EMNZ media ($\varepsilon, \mu \simeq 0$) and (*C*) a nonmagnetic dielectric material with the relative permittivity finely tuned to enable resonant transmission ($\varepsilon = 6.42$, $\mu = 1$). Those results were obtained by using a full-wave numerical solver (39).

that there are no sinks of power in lossless media; i.e., $\nabla \cdot \mathbf{S}_R = 0$. Interestingly, the imaginary part of Eq. **1** also vanishes in epsilon-and-mu-near-zero (EMNZ) media ($\mu', \varepsilon' \to 0$), for which the entire complex vector field $\mathbf{S}$ can be treated as a divergenceless (or solenoidal) quantity $\nabla \cdot \mathbf{S} = 0$.

Next, we use vector calculus identities to rewrite the curl of the Poynting vector field as follows:

$$\nabla \times \mathbf{S} = \frac{1}{2}\left[(\mathbf{H}^* \cdot \nabla)\mathbf{E} - (\mathbf{E} \cdot \nabla)\mathbf{H}^* + \mathbf{E}\,(\nabla \cdot \mathbf{H}^*) - \mathbf{H}^*\,(\nabla \cdot \mathbf{E})\right]. \qquad [2]$$

First, we have that outside the source region $\nabla \cdot \mathbf{E} = 0$ and $\nabla \cdot \mathbf{H} = 0$ except at the material boundaries. Second, we consider a 2D configuration with transverse magnetic (TM) polarization, i.e., $\mathbf{H} = \hat{\mathbf{z}}\, H_z(x, y)$ and $\mathbf{E} = \hat{\mathbf{x}}\, E_x(x, y) + \hat{\mathbf{y}}\, E_y(x, y)$, for which the first term in the right-hand side (r.h.s.) of Eq. **2** is zero. Finally, we note that the magnetic field in a 2D medium with a near-zero permittivity must be constant, $H_z(x, y) = H_z^{\mathrm{cst}}$, to avoid a divergent electric field, $\mathbf{E} = (-i\omega\varepsilon_0\varepsilon)^{-1}\nabla H_z \times \hat{\mathbf{z}}$, so that the second term in the r.h.s. of Eq. **1** also vanishes. Therefore it is found that $\nabla \times \mathbf{S} = \mathbf{0}$ for TM fields in all 2D media with a near-zero permittivity (i.e., epsilon-near-zero [ENZ] media), independently of the value of its permeability.

In other words, it can be concluded from Eqs. **1** and **2** that the complex Poynting vector field $\mathbf{S}$ for TM waves in 2D EMNZ media is characterized by the simple conditions $\nabla \cdot \mathbf{S} = 0$ and $\nabla \times \mathbf{S} = \mathbf{0}$. For an ENZ medium of arbitrary permeability μ, the same equations hold for the real part of the Poynting vector field (power flow); i.e., $\nabla \cdot \mathbf{S}_R = 0$ and $\nabla \times \mathbf{S}_R = \mathbf{0}$. Note that an identical reasoning for mu-near-zero (MNZ) ($\mu \simeq 0$) media leads to the same conclusions, for the transverse electric (TE) polarization. In addition, when the system is surrounded by opaque media (e.g., metallic mirrors in a waveguide), the boundary condition $\hat{\mathbf{n}} \cdot \mathbf{S} = 0$ must be satisfied, where $\hat{\mathbf{n}}$ is the unit vector normal to the boundary (Fig. 1*A*). Interestingly, these are exactly the equations of motion and boundary conditions for the velocity field $\mathbf{v}$ of an inviscid, incompressible, and irrotational fluid, often labeled as an ideal fluid (36–38).

The fluid dynamics in such a scenario are usually described by using two scalar fields, the velocity potential ϕ and the stream function ψ (36). First, since $\nabla \times \mathbf{S} = \mathbf{0}$, it is clear that the power flow can be described through a scalar potential $\mathbf{S} = \nabla\phi$, with $\mathbf{S}$ thus being perpendicular to the constant potential lines. Similarly, it is convenient to define $\mathbf{S} = \nabla \times (\hat{\mathbf{z}}\psi)$, such that $\mathbf{S}$ is parallel to the streamlines; i.e., $(\mathbf{S} \cdot \nabla)\psi = 0$. Note that ϕ and ψ have $W \cdot m^{-1}$ units in this context. Moreover, the electric-field distribution can be directly linked to the velocity potential and the stream function as $\mathbf{E} = -\left(H_z^{\mathrm{cst}*}\right)^{-1}\nabla \times (\hat{\mathbf{z}}\phi)$ and $\mathbf{E} = -\left(H_z^{\mathrm{cst}*}\right)^{-1}\nabla\psi$. Therefore, the electric field is parallel to the constant potential lines and perpendicular to the streamlines.

Both the velocity potential and the stream function are harmonic functions found as a solution to Laplace's equation; i.e., $\nabla^2\phi = 0$ and $\nabla^2\psi = 0$, subject to the boundary conditions $\partial\phi/\partial n = 0$ and $\partial\psi/\partial l = 0$, where $\hat{\mathbf{n}}$ and $\hat{\mathbf{l}}$ are the normal and tangential unit vectors to the surface of solid bodies, respectively (Fig. 1*A*). This description is highly convenient, since the flow of electromagnetic energy in 2D NZI systems can then be described through potential theory, for which many tools have been developed, including the construction of solution by means of the superposition of elementary functions, conformal mapping, and numerical methods (36–38, 40).

Revisiting Supercoupling as Ideal Fluid Flow

In the following, we use this theory to analyze different transmission and scattering configurations in 2D NZI media. First, we study how the power flow in a 2D NZI waveguide is modified when the waveguide walls are deformed (Fig. 2). As a case study, we model the waveguide deformation by introducing a 2D obstacle consisting of a semiellipse with major $a_y = a_1 + a_2^2/a_1$ and minor $a_x = a_1 - a_2^2/a_1$ axes characterized by the parameters a_1 and a_2. The potential and stream function in this configuration can be found in closed form via conformal mapping by taking the complex potential for a circular cylinder of radius a_1, $z + a_1^2/z$; applying an inverse rotation transformation, $z \to ze^{-i\pi/2}$; followed by an inverse Joukowski transformation, $z \to 1/2\,(z + \sqrt{z^2 - 4a_2^2})$; and then adding the contributions from the images on the waveguide walls (37). This calculation leads to a complex potential, whose real and imaginary parts correspond to the potential and stream function, respectively:

$$\phi(x, y) + i\,\psi(x, y) = -\frac{i}{2}\left\{z + \sqrt{z^2 - 4a_2^2} - \frac{a_1^2}{a_2^2}\sum_{n=-\infty}^{\infty}\left(z_n - \sqrt{z_n^2 - 4a_2^2}\right)\right\} \qquad [3]$$

with $z = x + iy$ and $z_n = z - n2h$.

Fig. 2*B* depicts the constant velocity potential (dashed blue) and stream function (black) lines, as calculated from Eq. **3**.

Downloaded at Tsinghua Univ Library on September 10, 2020

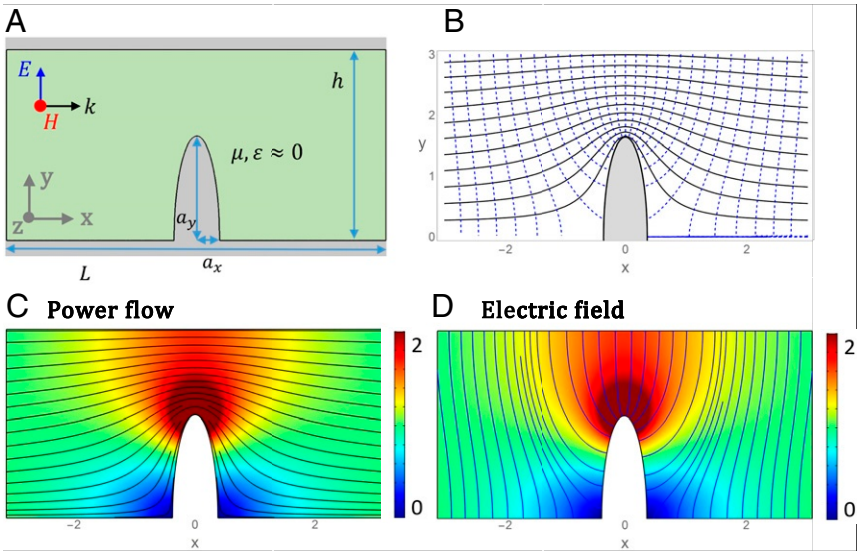

Fig. 2. (*A*) Sketch of the geometry: a 2D EMNZ waveguide of height $h = 3\lambda_p$ containing a deformed section modeled as a half-ellipse with semiaxes $a_y = a_1 + a_2^2/a_1$ and $a_x = a_1 - a_2^2/a_1$ with $a_1 = 2.5\lambda_p$ and $a_2 = 0.8\lambda_p$. All waveguide walls are considered as PEC boundaries, and λ_p is the free-space wavelength at the NZI frequency. (*B*) Constant potential lines (dashed blue) and streamlines (black) as obtained from the closed-form solution derived via conformal mapping. (*C* and *D*) Amplitude and streamlines of the (*C*) Poynting vector field and (*D*) electric field, normalized to their incident counterparts, as obtained with a full-wave electromagnetic solver (39).

As could be expected from an ideal fluid, the constant stream function lines smoothly go around the obstacle, no vorticity is observed, and the flow recovers its distribution as we move past the obstacle. Next, the same structure is analyzed by solving the electromagnetic problem with a full-wave numerical solver (39). Fig. 2 *C* and *D* reports the amplitude and streamlines of the Poynting vector field and electric field, respectively. By comparing the results it can be directly concluded that the streamlines for the electric and Poynting vector fields perfectly match those of the constant potential and stream function lines.

Therefore, these numerical simulations ratify that the power flow in deformed NZI waveguides mimics that of an ideal fluid. Consequently, we can state that deformations in NZI waveguides do not introduce any turbulent behavior. In addition, although the characteristics of this power flow have been theoretically derived in the zero-index limit (thus including the lossless limit), numerical simulations reveal that the lack of vorticity is very robust against the presence of loss (*SI Appendix*, Figs. S1 and S2). A similar effect is observed as the value of the real part of the permittivity and permeability deviates from zero, limiting the bandwidth in which this effect is observed, which critically depends on the size of the structure and the dispersion properties of the material parameters (*SI Appendix*, Fig. S3).

Scattering Configurations and Airfoil Theory

This theory can be applied to a large number of 2D scenarios, not necessarily restricted to waveguide configurations. Moreover, the possibility of using conformal mapping enables the analysis of complex geometries, while at the same time drawing interesting connections between NZI electrodynamics and different aspects of fluid dynamics such as airfoil theory (36–38). For example, Fig. 3 illustrates the power flow of a finite-size perfect electric conductor (PEC) 2D object immersed in an open EMNZ medium, whose cross-section matches that of a typical airfoil model. In particular, the surface of this object can be parametrically described as $x(\theta) + iy(\theta) = \frac{1}{2}\left[\alpha e^{i\theta} + \beta + \left(\alpha e^{i\theta} + \beta\right)^{-1}\right]$, with $\beta = 0.3\, e^{i0.65\pi}$, $\alpha = |1 - \beta|$, and θ ranging from 0 to 2π (36, 37). We assume that this object is in the presence of a uniform flow at an angle $\theta_0 = 10°$. In this case, a closed-form solution for the potential and stream functions can also be found using conformal mapping (36, 37). In particular, we start with the complex potential of a circle cylinder of radius α, i.e., $\phi + i\psi = z + \alpha^2/z$; and then apply an inverse rotation transform, $z \to ze^{-i\theta_0}$; followed by an inverse translation transform, $z \to z - \beta$; and finally

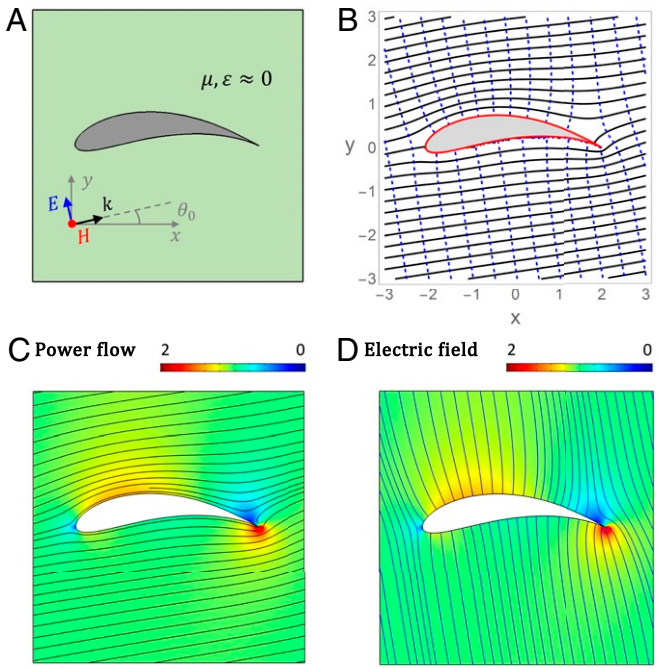

Fig. 3. (*A*) Sketch of the geometry: a PEC body, with a typical cross-section of an airfoil, immersed in an open EMNZ medium and illuminated by a plane wave with TM polarization. (*B*) Constant potential lines (dashed blue) and streamlines (black) as obtained from the closed-form solution derived via conformal mapping. (*C* and *D*) Amplitude and streamlines of the (*C*) Poynting vector field and (*D*) electric field, normalized to their incident counterparts, as obtained with a full-wave electromagnetic solver (39).

Downloaded at Tsinghua Univ Library on September 10, 2020

an inverse Joukowski transform $z \to \frac{1}{2}\left(z - \sqrt{z^2-4}\right)$ is carried out (40).

Fig. 3*B* depicts the constant velocity potential and stream function lines as computed from such a solution. Again, the flow around the object is characterized by a smooth transition avoiding the object, with no shadow, vorticity, or turbulence at the object edges. The flow is also characterized by two stagnation points where the streamlines are perpendicular to the surface of the object, and the velocity field is zero (36–38). Fig. 3 *C* and *D* depicts the Poynting vector-field and electric-field distributions, respectively. This example confirms how the power flow over objects immersed in NZI media, even with a complex geometry, can be readily analyzed via fluid mechanic tools.

The Role of the Permeability

Up to this point, all examples have focused on EMNZ media, for which both ε and μ are near zero. However, since most materials are nonmagnetic ($\mu = 1$) at optical frequencies, one should consider whether the role of the permeability is crucial in the behavior of NZI media as an electromagnetic ideal fluid. Indeed, EMNZ media and ENZ media with a nonzero value of the permeability present differing properties. For example, while both share a near-zero refractive index, $\sqrt{\mu(\omega_p)\varepsilon(\omega_p)} \to 0$, the medium impedance diverges in nonmagnetic ($\mu = 1$) ENZ media $Z(\omega_p) = 1/\sqrt{\varepsilon(\omega_p)} \to \infty$, while it converges to a finite value in EMNZ media, $Z(\omega_p) = \sqrt{\partial_\omega \mu(\omega_p)/\partial_\omega \varepsilon(\omega_p)}$. Similarly, ENZ media with a nonzero value of permeability, when lossless and infinitely extent, necessarily exhibit a near-zero group velocity, $v_g(\omega_p) \to 0$ (41), while EMNZ media exhibit a nonzero group velocity $v_g(\omega_p) = c/(\omega_p \partial_\omega \sqrt{\mu(\omega_p)\varepsilon(\omega_p)})$ (42). In passing, note that a near-zero group velocity in the unbounded lossless case does not prevent supercoupling phenomena, as it takes place in finite waveguide sections, and as it can also be shown in the time-domain analysis of the effect (43). With their different material properties, ENZ and EMNZ media also exhibit differing wave phenomena. For example, EMNZ supercoupling is observed for any waveguide geometry (44), while ENZ supercoupling is observed only in narrow channels in the limit in which the area of the waveguide goes to zero (5), albeit independently of the geometry in which this limit is approached.

Knowing these different material properties and wave dynamics, one should expect that the power flow distribution would be different as a function of the permeability of the ENZ medium. Remarkably, this is not the case. In particular, it can be shown that the power flow in ENZ and EMNZ media is identical up to a scalar factor. To demonstrate this point, we revisit Eqs. **1** and **2** and note that the power flow $\mathbf{S}_R = \mathrm{Re}[\mathbf{S}]$ in ENZ media ($\varepsilon \simeq 0$, $\mu \neq 0$) also obeys the equations of the velocity field of an ideal fluid $\nabla \cdot \mathbf{S}_R = 0$ and $\nabla \times \mathbf{S}_R = 0$. Mathematically, this conclusion can be drawn from the fact that the solutions to Laplace's equation are in such a way that they do not contain any material parameters. Therefore, those solutions are purely geometrical, depending only on the shape of the bodies and on the exciting fields. For the same reason, the distribution of the power flow $\mathbf{S}_R$ in ENZ media is independent of its relative permeability, up to a scalar factor (please refer to *SI Appendix*, Figs. S4–S6 for numerical examples illustrating this point). Specifically, this scalar factor is given by the squared magnitude of the constant magnetic field excited in the ENZ host, normalized to the incident field, i.e., $\left|H_z^{\mathrm{cst}}\right|^2$. The value of the magnetic field can be found by imposing Faraday's law on the NZI region: $H_z^{\mathrm{cst}} = \left(1 + i\frac{\omega}{c}\frac{A}{2h}\mu\right)^{-1}$, where A is the area of the deformed waveguide section. The value of this scalar factor determines the magnitude and phase of the transmitted and reflected waves and the different supercoupling effects observed in EMNZ and ENZ media.

Photonic Doping and Power Flow around Dielectric Particles

Aside from the examples above in which PEC boundaries have been considered (including waveguide walls, obstacles, and finite-size objects), there is much interest in the electromagnetic response of ENZ bodies containing dielectric particles (11). In fact, it has been found that a 2D ENZ medium goes beyond conventional effective medium theories, and dielectric particles immersed in it modify its effective permeability, while maintaining a near-zero permittivity. In addition, the contribution from each dielectric particle is additive (as if the particles were not interacting) and independent of the particles' positions. This represents a fundamentally different way of synthesizing artificial electromagnetic materials, usually referred to as photonic doping (11).

The theory introduced in this work can be used to clarify the power flow around dielectric particles acting as photonic dopants. Since the magnetic field of a TM wave in a 2D ENZ host is constant, the magnetic field inside a dielectric inclusion of area A_p and boundary ∂A_p can be written as $H_z(x,y) = H_z^{\mathrm{cst}}\,\xi_p(x,y)$, where ξ_p is the solution to the scalar Helmholtz equation, subject to the boundary condition $\xi_p = 1$ on ∂A_p. Consequently, the electric and Poynting vector fields are given by $\mathbf{E} = H_z^{\mathrm{cst}}(i\omega\varepsilon_0\varepsilon_p)^{-1}\hat{\mathbf{z}} \times \nabla\xi_p$ and $\mathbf{S} = \left|H_z^{\mathrm{cst}}\right|^2 (i2\omega\varepsilon_0\varepsilon_p)^{-1}\xi_p\nabla\xi_p$, respectively, where ε_p is the relative permittivity of the dielectric inclusion. Interestingly, for particles in which both ε_p and ξ_p are real, as is indeed the case for lossless particles, the Poynting vector field is purely imaginary within the particle. In other words, the power flow is identically zero within the particle, $\mathbf{S}_R = \mathbf{0}$. Consequently, the power flow distribution in an ENZ medium photonically doped with 2D dielectric particles is independent of the internal properties of the particles, except to a scalar factor, and it is purely determined by its external boundaries. This scalar factor is again $\left|H_z^{\mathrm{cst}}\right|^2$, with $H_z^{\mathrm{cst}} = \left(1 + i\frac{\omega}{c}\frac{A}{2h}\mu_{\mathrm{eff}}\right)^{-1}$, where A is the area of the ENZ host, and $\mu_{\mathrm{eff}} = 1 + \sum_p \Delta\mu_p$ with $\Delta\mu_p = A^{-1}\left[\int_{A_p} \xi_p(x,y)\,dA - A_p\right]$ is the effective permeability induced by the dielectric dopants (11).

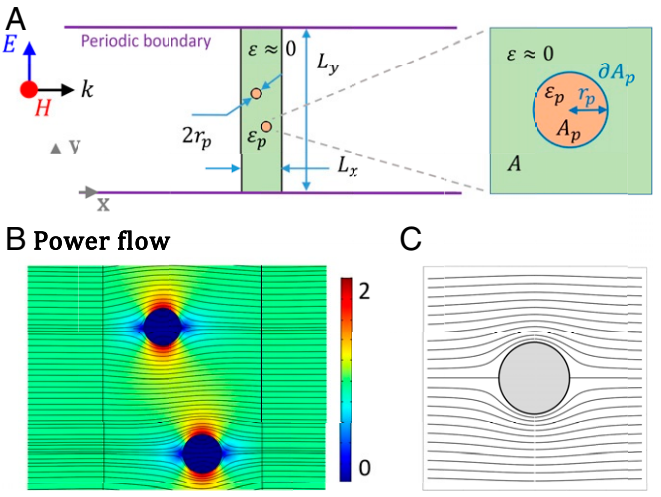

Fig. 4. (*A*) Sketch of the geometry: A nonmagnetic ENZ slab ($\varepsilon \simeq 0$, $\mu = 1$) of thickness $L_x = \lambda_p$ is periodically doped with two identical dielectric cylinders with a circular cross-section $A_p = \pi r_p^2$ with radius $r_p = 0.122\lambda_p$, bounded by the contour ∂A_p, and with relative permittivity $\varepsilon_p = 10$. The slab periodicity in the *y* axis is of $L_y = 2\lambda_p$. This configuration is excited under normal incidence by a plane-wave with TM polarization. (*B*) Amplitude and streamlines of the Poynting vector field (real part), normalized to the incident Poynting vector field obtained with a full-wave electromagnetic solver (39). (*C*) Streamlines obtained from the closed-form solution to the ideal fluid flow around a circular cylinder.

Downloaded at Tsinghua Univ Library on September 10, 2020

To illustrate this effect, Fig. 4 depicts the power flow within a metasurface composed of a 2D ENZ slab periodically doped by dielectric particles. The dopants consist of circular cylinders of radius r_p and relative permittivity ε_p, for which $\xi_p = J_0(k_p r)/J_0(k_p r_p)$, with $k_p = \omega/c\sqrt{\varepsilon_r}$. As anticipated, the power flow within the dielectric particles is zero. Outside the particles, the power flow corresponds to that of a perfect fluid flow around a circular cylinder, i.e., $\phi(x,y)+i\psi(x,y)=z+r_p^2/z$, despite the fact that the particles are dielectric.

Conclusions

Our formulation demonstrates that the power flow in 2D NZI media can be understood as analogous to that of an ideal fluid (inviscid, incompressible, and irrotational flow). We believe that this result provides additional insight and a better understanding of how NZI supercoupling takes place and why it is independent of the waveguide deformations. In addition, our results might trigger additional research by establishing further connections between the fields of fluid dynamics and NZI electrodynamics. In this regard, different effects and directions could be explored. For example, it is known that the drag of any body of any shape immersed in a uniform stream is identically zero (a result often referred to as the D'Alambert paradox). On the contrary, the lift, i.e., the force perpendicular to the stream, can be nonzero (Magnus–Robins force). These effects might have important implications on the optical forces induced in objects immersed in ENZ media. Beyond supercoupling, our theory might enable revisiting the power flow in other salient features of NZI media, including nonradiating eigenmodes (45–47), geometry-invariant resonant cavities (48), highly directive systems (6, 49, 50), and nonlinear phenomena (2, 51). Furthermore, viscosity is known to have a destabilizing effect on fluids, giving rise to disorderly, random flows, usually referred to as turbulence. Here, it is shown that NZI media give access to optical systems where turbulence is intrinsically inhibited, an effect that might offer interesting technological possibilities for optical systems operating under extreme mechanical conditions.

Data Availability. All study data are included in the article and in *SI Appendix*.

ACKNOWLEDGMENTS. I.L. acknowledges support from Ramón y Cajal Fellowship RYC2018-024123-I and Project RTI2018-093714-J-I00 sponsored by MCIU/AEI/FEDER/UE. N.E. acknowledges partial support from the Vannevar Bush Faculty Fellowship program sponsored by the Basic Research Office of the Assistant Secretary of Defense for Research and Engineering and funded by the Office of Naval Research through Grant N00014-16-1-2029.

1. I. Liberal, N. Engheta, Near-zero refractive index photonics. *Nat. Photonics* **11**, 149–158 (2017).
2. O. Reshef, I. De Leon, M. Z. Alam, R. W. Boyd, Nonlinear optical effects in epsilon-near-zero media. *Nat. Rev. Mater.* **4**, 535–551 (2019).
3. N. Kinsey, C. DeVault, A. Boltasseva, V. M. Shalaev, Near-zero-index materials for photonics. *Nat. Rev. Mater.* **4**, 742–760 (2019).
4. D. I. Vulis, O. Reshef, P. Camayd-Muñoz, E. Mazur, Manipulating the flow of light using Dirac-cone zero-index metamaterials. *Rep. Prog. Phys.* **82**, 012001 (2018).
5. M. Silveirinha, N. Engheta, Tunneling of electromagnetic energy through subwavelength channels and bends using ε-near-zero materials. *Phys. Rev. Lett.* **97**, 157403 (2006).
6. R. W. Ziolkowski, Propagation in and scattering from a matched metamaterial having a zero index of refraction. *Phys. Rev. E* **70**, 046608 (2004).
7. I. Liberal, N. Engheta, Zero-index platforms: Where light defies geometry. *Opt. Photonics News* **27**, 26–33 (2016).
8. B. Edwards, A. Alu, M. E. Young, M. Silveirinha, N. Engheta, Experimental verification of epsilon-near-zero metamaterial coupling and energy squeezing using a microwave waveguide. *Phys. Rev. Lett.* **100**, 033903 (2008).
9. B. Edwards, A. Alu, M. G. Silveirinha, N. Engheta, Reflectionless sharp bends and corners in waveguides using epsilon-near-zero effects. *J. Appl. Phys.* **105**, 044905 (2009).
10. J. S. Marcos, M. G. Silveirinha, N. Engheta, μ-near-zero supercoupling. *Phys. Rev. B* **91**, 195112 (2015).
11. I. Liberal, A. M. Mahmoud, Y. Li, B. Edwards, N. Engheta, Photonic doping of epsilon-near-zero media. *Science* **355**, 1058–1062 (2017).
12. E. J. R. Vesseur, T. Coenen, H. Caglayan, N. Engheta, A. Polman, Experimental verification of n = 0 structures for visible light. *Phys. Rev. Lett.* **110**, 013902 (2013).
13. X. Huang, Y. Lai, Z. H. Hang, H. Zheng, C. Chan, Dirac cones induced by accidental degeneracy in photonic crystals and zero-refractive-index materials. *Nat. Mater.* **10**, 582–586 (2011).
14. O. Reshef *et al.*, Direct observation of phase-free propagation in a silicon waveguide. *ACS Photonics* **4**, 2385–2389 (2017).
15. J. Luo, B. Liu, Z. H. Hang, Y. Lai, Coherent perfect absorption via photonic doping of zero-index media. *Laser Photonics Rev.* **12**, 1800001 (2018).
16. Z. Zhou *et al.*, Substrate-integrated photonic doping for near-zero-index devices. *Nat. Commun.* **10**, 4132 (2019).
17. C. Argyropoulos, P. Y. Chen, G. D'Aguanno, N. Engheta, A. Alu, Boosting optical nonlinearities in ε-near-zero plasmonic channels. *Phys. Rev. B* **85**, 045129 (2012).
18. C. Argyropoulos, G. D'Aguanno, A. Alu, Giant second-harmonic generation efficiency and ideal phase matching with a double ε-near-zero cross-slit metamaterial. *Phys. Rev. B* **89**, 235401 (2014).
19. A. Alu, N. Engheta, Dielectric sensing in ϵ-near-zero narrow waveguide channels. *Phys. Rev. B* **78**, 045102 (2008).
20. J. C. Soric, N. Engheta, S. Maci, A. Alu, Omnidirectional metamaterial antennas based on ε-near-zero channel matching. *IEEE Trans. Antennas Propag.* **61**, 33–44 (2012).
21. J. C. Soric, A. Alù, Longitudinally independent matching and arbitrary wave patterning using ε-near-zero channels. *IEEE Trans. Microw. Theory Tech.* **63**, 3558–3567 (2015).
22. M. Memarian, G. V. Eleftheriades, Dirac leaky-wave antennas for continuous beam scanning from photonic crystals. *Nat. Commun.* **6**, 5855 (2015).
23. V. Pacheco-Peña, V. Torres, M. Beruete, M. Navarro-Cía, N. Engheta, Near-zero (ENZ) graded index quasi-optical devices: Steering and splitting millimeter waves. *J. Optics* **16**, 094009 (2014).
24. V. Pacheco-Peña *et al.*, Mechanical 144 GHz beam steering with all-metallic epsilon-near-zero lens antenna. *Appl. Phys. Lett.* **105**, 243503 (2014).
25. A. Alu, N. Engheta, Boosting molecular fluorescence with a plasmonic nanolauncher. *Phys. Rev. Lett.* **103**, 043902 (2009).
26. R. Sokhoyan, H. A. Atwater, Quantum optical properties of a dipole emitter coupled to an ϵ-near-zero nanoscale waveguide. *Opt. Express* **21**, 32279–32290 (2013).
27. R. Fleury, A. Alu, Enhanced superradiance in epsilon-near-zero plasmonic channels. *Phys. Rev. B* **87**, 201101 (2013).
28. Y. Li, C. Argyropoulos, Controlling collective spontaneous emission with plasmonic waveguides. *Opt. Express* **24**, 26696–26708 (2016).
29. A. Mahmoud, I. Liberal, N. Engheta, Dipole-dipole interactions mediated by epsilon-and-mu-near-zero waveguide supercoupling. *Opt. Mater. Express* **7**, 415–424 (2017).
30. E. Özgün, E. Ozbay, H. Caglayan, Tunable zero-index photonic crystal waveguide for two-qubit entanglement detection. *ACS Photonics* **3**, 2129–2133 (2016).
31. I. Liberal, N. Engheta, Multiqubit subradiant states in n-port waveguide devices: ε-and-μ-near-zero hubs and nonreciprocal circulators. *Phys. Rev. A* **97**, 022309 (2018).
32. R. Fleury, A. Alu, Extraordinary sound transmission through density-near-zero ultranarrow channels. *Phys. Rev. Lett.* **111**, 055501 (2013).
33. H. Esfahlani, M. Byrne, M. McDermott, A. Alu, Acoustic supercoupling in a zero-compressibility waveguide. *Research* **2019**, 1–10 (2019).
34. R. Fleury, A. Alu, Manipulation of electron flow using near-zero index semiconductor metamaterials. *Phys. Rev. B* **90**, 035138 (2014).
35. R. E. Collin, *Field Theory of Guided Waves* (McGraw-Hill, 1960).
36. F. M. White, *Fluid Mechanics* (McGraw-Hill Education, 2015).
37. D. J. Acheson, *Elementary Fluid Dynamics* (Oxford University Press, 1991).
38. W. S. Janna, *Introduction to Fluid Mechanics* (CRC Press, 2015).
39. Comsol Multiphysics, Wave Optics Module. https://www.comsol.com. Accessed 30 August 2020.
40. R. L. Fearn, Airfoil aerodynamics using panel methods. https://content.wolfram.com/uploads/sites/19/2008/11/PanelMethods.pdf. Accessed 30 August 2020.
41. M. H. Javani, M. I. Stockman, Real and imaginary properties of epsilon-near-zero materials. *Phys. Rev. Lett.* **117**, 107404 (2016).
42. M. Lobet *et al.*, Fundamental radiative processes in near-zero-index media of various dimensionalities. *ACS Photonics* **7**, 1965–1970 (2020).
43. I. Liberal, Y. Li, N. Engheta, Reconfigurable epsilon-near-zero metasurfaces via photonic doping. *Nanophotonics* **7**, 1117–1127 (2018).
44. A. M. Mahmoud, N. Engheta, Wave-matter interactions in epsilon-and-mu-near-zero structures. *Nat. Commun.* **5**, 5638 (2014).
45. M. G. Silveirinha, Trapping light in open plasmonic nanostructures. *Phys. Rev. A* **89**, 023813 (2014).
46. F. Monticone, A. Alu, Embedded photonic eigenvalues in 3d nanostructures. *Phys. Rev. Lett.* **112**, 213903 (2014).
47. I. Liberal, N. Engheta, Nonradiating and radiating modes excited by quantum emitters in open epsilon-near-zero cavities. *Sci. Adv.* **2**, e1600987 (2016).
48. I. Liberal, A. M. Mahmoud, N. Engheta, Geometry-invariant resonant cavities. *Nat. Commun.* **7**, 10989 (2016).
49. S. Enoch, G. Tayeb, P. Sabouroux, N. Guérin, P. Vincent, A metamaterial for directive emission. *Phys. Rev. Lett.* **89**, 213902 (2002).
50. A. Alu, M. G. Silveirinha, A. Salandrino, N. Engheta, Epsilon-near-zero metamaterials and electromagnetic sources: Tailoring the radiation phase pattern. *Phys. Rev. B* **75**, 155410 (2007).
51. S. Lannebère, M. G. Silveirinha, Optical meta-atom for localization of light with quantized energy. *Nat. Commun.* **6**, 8766 (2015).

Downloaded at Tsinghua Univ Library on September 10, 2020